Exciton Bose–Einstein Condensation in Transition Metal Dichalcogenide Monolayer under In-Plane Magnetic Fields

Dengfeng Wang(王登峰)[1,2†], Yingda Chen(陈颖达)[1,2†], Zhi-Chuan Niu(牛智川)[1,2], Wen-Kai Lou(娄文凯)[1,2*], and Kai Chang(常凯)[1,2,3*]

[1]*SKLSM, Institute of Semiconductors, Chinese Academy of Sciences, Beijing 100083, China*
[2]*College of Materials Science and Opto-electronic Technology, Center of Materials Science and Optoelectronics Engineering, University of Chinese Academy of Sciences, Beijing 100049, China*
[3]*School of Physics, Zhejiang University, Hangzhou 310027, China*

(Received 20 April 2024; accepted manuscript online 4 July 2024)

Based on the Gross–Pitaevskii equation, we theoretically investigate exciton Bose–Einstein condensation (BEC) in transition metal dichalcogenide monolayers (TMDC-MLs) under in-plane magnetic fields. We observe that the in-plane magnetic fields exert a strong influence on the exciton BEC wave functions in TMDC-MLs because of the mixing of the bright and dark exciton states via Zeeman effect. This leads to the brightening of the dark exciton BEC states. The competition between the dipole–dipole interactions caused by the long-range Coulomb interaction and the Zeeman effect induced by the in-plane magnetic fields can effectively regulate dark exciton BEC states. Our findings emphasize the utility of TMD-MLs as platforms for investigating collective phenomenon involving excited states.

DOI: 10.1088/0256-307X/41/8/087101

Bose–Einstein condensation (BEC) is a macroscopic quantum phenomenon of identical bosons,[1,2] leading to many fantastic properties, such as superconductivity[3] and superfluidity.[4] About thirty years ago, Anderson *et al.* performed the first experimental observation of BEC in cold rubidium atoms (^{87}Rb) at 170 nK.[5] This groundbreaking discovery has opened a door to the further research on BEC and its practical applications in quantum information and computation techniques.

BEC can be realized in many specific materials, such as cold atoms[6] and quantum magnets.[7] In cold atom systems, obtaining enough atoms into BEC states requires extremely low temperature due to large atomic mass. To achieve a higher transition temperature for particles to enter BEC states, it is essential to consider Bosons with smaller mass and higher concentration. The exciton systems possess both the advantages. Furthermore, the interaction between two excitons involves long-range electric dipole–dipole interactions (DDIs) and appears naturally in exciton gases, providing us rich quantum phenomena and quantum phases.

Early studies on the exciton BEC systems are primarily focused on coupled quantum wells.[8–11] The electron–hole separation induced by specific electric fields can enhance lifetime of excitons.[10] However, the BEC transition temperature is still very low due to small exciton binding energy about a few meV. The recent explosive development of two-dimensional (2D) materials has opened new avenues to explore exciton physics. In these materials, the binding energy of excitons is significantly enhanced, even to 1 eV,[12,13] because of weak screening effect,[13] which greatly enhances the Coulomb attraction between electrons and holes. Additionally, the movement of excitons in the vertical direction is greatly limited. As a result, these excitons in 2D materials may condense at higher temperature.[14,15]

The bulk 2D transition metal dichalcogenides (TMDCs) have unique optical and photoelectric properties[16] since their strong spin orbit coupling[17,18] and finite band gap.[19] As the bulk TMDCs transition into the single-layer limit, the quantum confinement effect becomes stronger. Simultaneously, the band structure in TMDCs transitions from an indirect band gap in the bulk materials to a direct band gap in TMDC monolayers (TMDC-MLs) at K/K' points.[20,21] This physical effect greatly improves the response of the optical transition and photoluminescence, resulting in ultra-narrow half width peaks in optical spectra, which are not typically observed in bulk materials. Therefore, this class of materials has wide applications in photonics and optoelectronics due to the significant exciton effect.

In TMDC-MLs, the ground state of excitons can exhibit bright (dark) states,[22] which allows (forbids) for the parallel spin configurations between the top valence band (VB) and the lowest conduction band (CB). Conventionally, dark excitons are a type of quasiparticle which are not easy to observe due to their low luminescent intensity. A few experimental works have reported the observation of dark excitons, revealing that dark excitons can possess long exciton lifetime ($\tau_{\rm d} = 59$ ms[23]) in WSe_2

†These authors contributed equally to this work.
*Corresponding authors. Email: wklou@semi.ac.cn; kchang@semi.ac.cn
© 2024 Chinese Physical Society and IOP Publishing Ltd

monolayers and can be experimentally detected in different systems.[24–26] Dark exciton BEC states have been rarely reported before due to the optical inactivity. However, bright excitons have stronger optical activity but much shorter lifetime (only a few picoseconds[23]), and can only survive for short period with laser pumping. Therefore, experiments of realizing bright exciton BEC states are also very challenging.

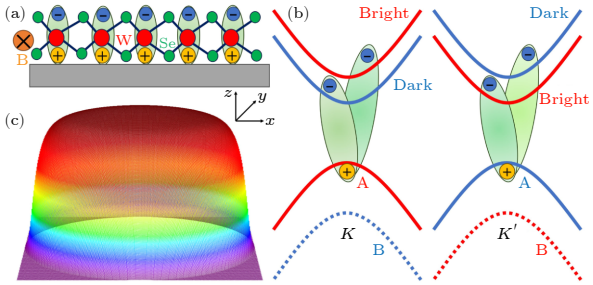

Fig. 1. Bright and dark excitons in TMDC-MLs under in-plane magnetic fields. (a) Schematics diagram of excitons in a WSe_2 ML under an in-plane magnetic field. The red circle indicates the tungsten atoms, the green circle shows the selenium atom, and the plus (minus) symbols represent the holes (electrons). The in-plane magnetic field is parallel the xy plane. (b) Schematics diagram of the bright/dark and A/B exciton states at the K/K' valleys. The red and blue bands mean different spin components. The red bands represent spin-up, and the blue bands represents spin-down. (c) The typical wavefunction of the exciton BEC states under an in-plane magnetic field.

An intriguing problem is how to effectively observe exciton BEC states by utilizing the optical activity of bright excitons and the longer lifetime of dark excitons. It is easy to imagine that if one can combine the advantages of bright and dark excitons, the realization of the BEC states may become easier. In our previous work, we employed a vertical electric field to mix bright and dark exciton states, and realized exciton BEC states and vortex states in WSe_2.[27] In that work, the vertical electric field induces electron–hole separation in real space and extends the exciton lifetime. Additionally, the Rashba-type $SU(2)$ gauge field induced by the vertical electric field couples the bright and dark exciton BEC states.[27] Interestingly, many works recently reported that the in-plane magnetic fields can greatly enhance the brightness of dark excitons and increase their observability.[28–36]

Over the decades, the in-plane magnetic fields have been employed to enhance the spectroscopy of dark excitons, such as in bulk semiconductors[30] and semiconductor quantum dots.[31] Recently, this concept has been applied to the TMDC-MLs,[28,32–36] because the in-plane magnetic fields mix the two lowest spin levels in the CB to bright the dark excitons.[29] That is to say, the optical transition becomes spin-permitted from spin-forbidden. However, these works involving in-plane magnetic fields are only focused on the optical properties, with little attention to the exciton correlation effect and exciton BEC states.

In the present work, we focus on the exciton BEC states of the TMDC-MLs under in-plane magnetic fields. We focus on the exciton condensation in BEC form rather than excitonic insulators.[37,38] We find that the in-plane magnetic fields mix the two spin levels in CB due to Zeeman effect and have greatly impact on the exciton BEC states in TMDC-MLs. When the in-plane magnetic fields are introduced, the bright exciton BEC states induce notable optoelectronic activity within the dark exciton BEC states. Consequently, this leads to the illumination of the dark exciton BEC states across all examined systems, such as MoS_2, $MoSe_2$, WS_2, and WSe_2 under in-plane magnetic fields. Our work can enrich the way of realization of exciton BEC states.

In this Letter, first we derive the Hamiltonian of exciton BEC states in TMDC-MLs under in-plane magnetic fields. The effective dielectric function with the Keldysh approximation and the interface traps are also taken into account. The coupled Gross–Pitaevskii (GP) equations including the DDI term between excitons are also derived. Then, we solve the GP equations using the imaginary time propagation method and discuss the numerical results. Finally, we summarize our findings.

Model. In this work, we investigate the exciton BEC states in TMDC-MLs under in-plane magnetic fields, as depicted in Fig. 1(a). In order to describe the motions of the exciton BEC states, we consider non-interacting exciton states of TMDC-MLs[27] under an in-plane magnetic field $B = (B_x, B_y)$[28] with the form:

$$H_{\rm B} = \frac{1}{2} g_{\rm cb} \mu_{\rm B} (\sigma_x B_x + \sigma_y B_y), \tag{1}$$

where $g_{\rm cb}$ is the in-plane gyro-magnetic ratio, $\mu_{\rm B}$ is the Bohr magneton, and σ_x, σ_y are the Pauli matrixes. The elements of the in-plane magnetic field read $B_x \pm iB_y = B_0 e^{\pm i\theta}$, with $B_0 = \sqrt{B_x^2 + B_y^2}$, $\theta = \arctan(B_y/B_x)$. Since experimentalists usually observe the amplitude of density distribution rather than phase, in this work we focus on the impact of the amplitude of the in-plane magnetic field B_0 on the exciton BEC and set $\theta = 0$ for simplicity. To simplify the description of the exciton BEC systems, we neglect the valley coupling and the Rashba spin-orbit interaction between A and B excitons at low temperature, as shown in Fig. 1(b). In this approximation, the decoupling between A and B excitons enables us to focus solely on the A excitons due to the fact that the band-splitting of the valence band is far greater than the band-splitting of the conduction band, e.g., $\Delta_{\rm so,\,vb} \gg \Delta_{\rm so,\,cb}$. Therefore, the spin mixing in the VB can be neglected.[28] We focus on the lowest A excitons at K valley. The Hamiltonian of excitons can be expressed as a 2×2 matrix:[27,28]

$$H_{\rm ex} = \begin{pmatrix} H_{\rm kb} + \Delta_{\rm b} + V(r_{\rm e} - r_{\rm h}) & \frac{1}{2} g_{\rm cb} \mu_{\rm B} B_0 \\ \frac{1}{2} g_{\rm cb} \mu_{\rm B} B_0 & H_{\rm kd} + \Delta_{\rm d} + V(r_{\rm e} - r_{\rm h}) \end{pmatrix}, \tag{2}$$

where the kinetic energies of the bright and dark exciton BEC states are given by

$$\begin{aligned} H_{\rm kb} &= -\hbar^2 \nabla_{\rm e}^2 / 2m_{\rm e1} - \hbar^2 \nabla_{\rm h}^2 / 2m_{\rm h1}, \\ H_{\rm kd} &= -\hbar^2 \nabla_{\rm e}^2 / 2m_{\rm e2} - \hbar^2 \nabla_{\rm h}^2 / 2m_{\rm h1}. \end{aligned} \tag{3}$$

The two conduction band electron masses are m_{e1} and m_{e2}, the hole mass is m_{h1}, the band gap of the bright (dark) states is Δ_b (Δ_d), and $V(r_e - r_h)$ is the electron–hole interaction. We can see that the in-plane magnetic field B_0 is applied parallel to the plane of the TMDC monolayer, which mixes the bright and dark excitons.

Since the difference of the effective masses of the spin-splitting conduction band ($m_{e1} \neq m_{e2}$), we need to derive the average of electron mass $m_e = (m_{e1} + m_{e2})/2$, the mass difference $\delta m = (m_{e2} - m_{e1})/2$, and the hole mass $m_h = m_{h1}$. Then we introduce the center-of-mass $M = m_e + m_h$, the reduced mass $\mu = m_e m_h/M$, the center-of-mass motions $R = (m_e r_e + m_h r_h)/(m_e + m_h)$, and the relative motions $r = r_e - r_h$. The exciton relative motion and the center-of-mass motion are decoupled since $\delta m \ll M$. To simplify, we focus on the exciton center-of-mass motions by considering the Hamiltonian expressed as [27,28]

$$H_{ex} = \begin{pmatrix} -\frac{\hbar^2\nabla_R^2}{2M_b} - \frac{\Delta_{bd}}{2} & \frac{1}{2}g_{cb}\mu_B B_0 \\ \frac{1}{2}g_{cb}\mu_B B_0 & -\frac{\hbar^2\nabla_R^2}{2M_d} + \frac{\Delta_{bd}}{2} \end{pmatrix} + E_0. \quad (4)$$

Here, the effective masses of the bright and dark excitons are $M_b = M(1 - \delta m/m_e)$ and $M_d = M(1 + \delta m/m_e)$. The energy difference between bright and dark exciton states can be expressed as $\Delta_{bd} \equiv E_d - E_b = \Delta_d - \Delta_b + \varepsilon_d - \varepsilon_b$, with ε_d and ε_b given by the exciton relative motion equation [27]

$$\Big[-\frac{\hbar^2\nabla_r^2}{2\mu_{b(d)}} + V(r)\Big]\Phi_{b(d)}(r) = \varepsilon_{b(d)}\Phi_{b(d)}(r), \quad (5)$$

where the effective reduced mass of bright and dark excitons $\mu_b = \mu(1 - \delta m/m_e)$ and $\mu_d = \mu(1 + \delta m/m_e)$. In this work, we set the zero point of the exciton energy: $E_0 \equiv (E_b + E_d)/2 = (\Delta_b + \Delta_d)/2 + (\varepsilon_b + \varepsilon_d)/2$.

Next, we derive the model of the DDI term between excitons. [39] The Keldysh model can accurately describe the dielectric function. Thus, we can obtain the effective coulomb interaction using the Keldysh approximation and the DDI of excitons. Taking the thin-film limit $|Q|d \ll 1$ (d is the thickness of the TMDC-MLs), the DDI in the momentum space can be written as [27]

$$V_{dd}(Q) \equiv \frac{e^2 d}{\varepsilon_0 \varepsilon} \frac{1 + Qd[(\coth\eta_1 + \coth\eta_2) + \frac{1}{2}]}{1 + Qd[\coth(\eta_1 + \eta_2) + 1]}, \quad (6)$$

where $\eta_{1,2} = \frac{1}{2}\ln(\varepsilon + \varepsilon_{1,2})/(\varepsilon - \varepsilon_{1,2})$. The scattering processes of excitons mediated by the DDI in real space are described by

$$H_{dd} \equiv V_{dd}(R) * (|\psi_b(R)|^2 + |\psi_d(R)|^2), \quad (7)$$

where the asterisk (symbol) $*$ denotes the convolution operator. [27]

We then suppose an infinite circular quantum confinement for the bright and dark excitons: [27]

$$H_v = V_0\Theta(R - R_0), \quad V_0 \to \infty. \quad (8)$$

Combining Eqs. (4), (7), and (8), the exciton BEC states can be well described by the coupled GP equations

$$i\hbar\frac{\partial}{\partial t}\begin{pmatrix}\psi_b \\ \psi_d\end{pmatrix} = \begin{pmatrix} H_b - \frac{\Delta_{bd}}{2} & \frac{1}{2}g_{cb}\mu_B B_0 \\ \frac{1}{2}g_{cb}\mu_B B_0 & H_d + \frac{\Delta_{bd}}{2}\end{pmatrix}\begin{pmatrix}\psi_b \\ \psi_d\end{pmatrix}, \quad (9)$$

with

$$H_b = H_{Tb} + H_v + H_{dd}, \quad H_{Tb} = -\hbar^2\nabla_R^2/2M_b,$$
$$H_d = H_{Td} + H_v + H_{dd}, \quad H_{Td} = -\hbar^2\nabla_R^2/2M_d. \quad (10)$$

The average density of bright exciton BEC states can be independently controlled by the laser pumping. To simplify the problem, we can assume that both bright and dark exciton BEC states have an equal concentration. With a fixed average density of the bright and dark excitons, the static coupled GP equations can be simplified to

$$\begin{pmatrix} H_b - \frac{\Delta_{bd}}{2} & \frac{1}{2}g_{cb}\mu_B B_0 \\ \frac{1}{2}g_{cb}\mu_B B_0 & H_d + \frac{\Delta_{bd}}{2}\end{pmatrix}\begin{pmatrix}\psi_b \\ \psi_d\end{pmatrix} = \mu\begin{pmatrix}\psi_b \\ \psi_d\end{pmatrix}. \quad (11)$$

We solve Eqs. (11) with the boundary condition determined by Eq. (8), i.e., $(\psi_b, \psi_d)|_{R=R_0} = 0$ to obtain the exciton BEC ground states.

Numerical Solutions and Discussions. The stationary solution to Eqs. (11) can be solved through the imaginary time propagation accompanied by a normalization step (see the Supplementary Material for details). This method is extensively used in the ground-state calculations of BEC systems. [40–48] In our study, we consider excitons that are trapped within a localized nanoflake of TMDC monolayer, whose ground state can be depicted by the local minimum of energy evolved from a wave packet possessing no singularity (Gaussian typically). Here, without loss of generality, we consider a Gaussian wave packet as the initial wave function to solve the GP equation.

Excitons can be condensed in either BEC or BCS manner. Here, the exciton density is $10^{10}\,\mathrm{cm}^{-2}$ and the system studied is an exciton condensation in BEC form. The lifetime of excitons is much longer than the thermalization time. Therefore, it can be considered that excitons are in a relatively stable metastable state at this time, and it has enough time to form a BEC state. Once the BEC state is formed, it is the ground state with the lowest energy of the system, namely a many-body ground state with long life time.

To simplify, we take the WSe_2 ML as a typical example to illustrate the exciton BEC in TMDC-MLs (other TMDC-MLs will discuss in detail later). The two conduction band electron masses are $m_{e1} = 0.29m_0$ and $m_{e2} = 0.40m_0$, the hole mass is $m_{h1} = 0.36m_0$ (m_0 is the electron rest mass), [49] and the bright-dark splitting $\Delta_{bd} = -37\,\mathrm{meV}$. [49] The dielectric constants of the substrates (assumed vacuum) are chosen as $\varepsilon_{1,2} = 1.0$, and the WSe_2 ML is $\varepsilon = 4\pi\chi_{2D}/d$ with the 2D polarizability $\chi_{2D} = 7.18\,\text{Å}$. [50] Finally, we choose the average densities of bright (dark) excitons $n_{b(d)} = 10^{10}\,\mathrm{cm}^{-2}$ and the radius of this flake $R_0 = 0.3\,\mu\mathrm{m}$. We focus on the nondiagonal terms of the Hamiltonian in Eqs. (11) as follows:

$$H_{bd} = H_{db}^* = \frac{1}{2}g_{cb}\mu_B B_0 \int dR\psi_b^*(R)\psi_d(R). \quad (12)$$

We can see that the nondiagonal term $\int dR\psi_{\rm b}^{*}(R)\psi_{\rm d}(R)$ mixes the bright and dark exciton BEC states. We suppose the wave function $\psi=\sqrt{\rho}e^{i\varphi}$ ($\rho=|\psi|^2$) and put this in Eqs. (12), then we get

$$H_{\rm bd}=H_{\rm db}^{*}=\frac{1}{2}g_{\rm cb}\mu_{\rm B}B_0\int dR\sqrt{\rho_{\rm b}(R)\rho_{\rm d}(R)}e^{i(\varphi_{\rm b}-\varphi_{\rm d})}. \tag{13}$$

Now we can see the interference terms[51] between the bright and dark states with the in-plane magnetic fields at the right side of the integration of Eq. (13). Based on the numerical calculations of Eqs. (11), we find that the interaction of mixing plays an important role in the ground BEC states, as shown in Fig. 1(c) with a 0.8 T in-plane magnetic field. The magnetic length of the maximum magnetic field (0.8 T) is 28.68 nm, which is much larger than the thickness d (0.34 nm) of a single layer of 2D material when we consider it. Thus in this work, we ignore the orbital effect of the magnetic fields and only consider the Zeeman effect of the magnetic fields.

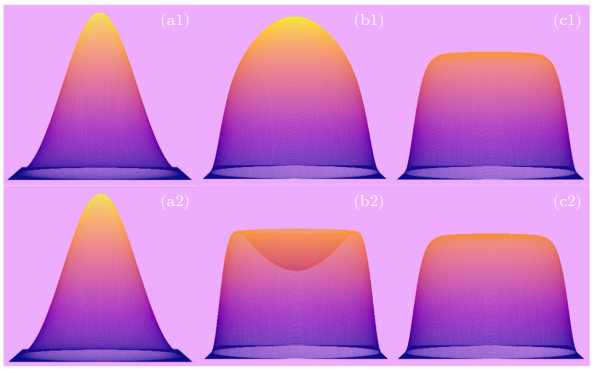

Fig. 2. Numerical results of the bright and dark exciton BEC states at K valley in a WSe_2 ML. We show the normalized density $\eta=\rho/N$ profiles of bright excitons (first line) and dark excitons (second line). [(a1), (a2)] The exciton BEC states without DDI. [(b1), (b2)] Adding the DDI term. [(c1), (c2)] Adding an in-plane magnetic field $B_0=0.80$ T. The radius of the WSe_2 ML is $R_0=0.3$ μm, and the fixed average densities of bright and dark exciton BEC states are $n_{\rm b(d)}=10^{10}\,{\rm cm}^{-2}$.

First of all, we investigate the effects of the DDI term [Eq. (7)] and the in-plane magnetic field [Eq. (12)] on the ground states of both bright and dark exciton BEC states. To illustrate how the DDI term and the in-plane magnetic field significantly influence the ground states of exciton BECs, as shown in Fig. 2, we present the density distributions under three distinct conditions: (I) No DDI and no magnetic field are present. (Ⅱ) DDI exists, but no magnetic field is present. (Ⅲ) Both DDI and magnetic field are present. For the case I, we observe that the density distributions without the DDI term resemble the same circular cone in both the bright and dark exciton BEC states, as shown in Figs. 2(a1) and 2(a2). The bright state and the dark state initially manifest as Gaussian wave packets, evolving independently without correlation between them.

When we incorporate the DDI term into the exciton BEC system, the wave function expands, indicating that the DDI potential is repulsive, as shown in Figs. 2(b1) and 2(b2). However, we find that the density distributions in the bright and dark exciton BEC states are distinct. In the bright state, the density distribution is convex, while in the dark state, it is concave, which is opposite to the bright state, due to the polarization of the DDI term. The in-plane magnetic field can couple the bright and dark exciton wave functions, mitigating the distribution differences between bright and dark exciton BEC states within the exciton BEC system, as shown in Figs. 2(c1) and 2(c2). This bright-dark exciton coupling leads to a brightening of the dark exciton states, facilitating the observation of dark exciton BEC states.

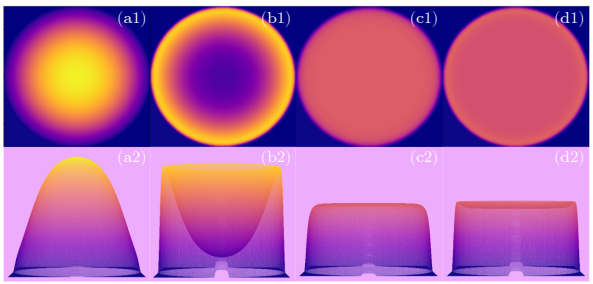

Fig. 3. Influence of the strength of the DDI on the bright and dark exciton BEC states at the K valley in a WSe_2 ML, induced by different densities of excitons. We show the normalized density $\eta=\rho/N$ (first line) and the density profiles (second line) of bright excitons [(a1), (a2), (c1), (c2)] and dark excitons [(b1), (b2), (d1), (d2)]. We set the different strengths of the in-plane magnetic fields $B_0=0.00$ T [(a1), (a2), (b1), (b2)] and $B_0=0.80$ T [(c1), (c2), (d1), (d2)]. The fixed average densities of bright and dark exciton BEC states are $n_{\rm b(d)}=20\times10^{10}\,{\rm cm}^{-2}$. The radius of the WSe_2 ML is $R_0=0.3$ μm.

Secondly, we investigate the influence of the stronger DDI term on the exciton BEC states, as illustrated in Fig. 3. The intensity of the DDI is directly proportional to the average density of excitons, so we primarily focus on the average density of exciton BEC states. In Fig. 3, we set $n_{\rm b(d)}=20.0\times10^{10}\,{\rm cm}^{-2}$, which is significantly higher than the density in Fig. 2. Comparing the exciton BEC states in Fig. 3 with those in Fig. 2, we observe a similar trend of variation. In the absence of an in-plane magnetic field, we can see that the hole in the dark exciton states, as shown in Fig. 3(b2), is much deeper than in Fig. 3(b2), since the stronger DDI produces larger repulsive interactions. Nevertheless, when the in-plane magnetic field appears, both the bright and dark exciton BEC states tend to average out, and the dark exciton BEC states become brighter. The competition between the DDI arising from the long-range Coulomb interaction and the Zeeman effect induced by the in-plane magnetic field can effectively regulate the formation of dark exciton BEC. In other words, this competitive mechanism allows us to utilize exciton concentration and in-plane magnetic fields to adjust the strength of the dark exciton BEC state.

If we vary the average densities of the bright and dark exciton BEC states, as shown in Figs. 4(a), 4(b), 4(e), and 4(f) with $n_{\rm b}=3n_{\rm d}=3\times10^{10}\,{\rm cm}^{-2}$, and in Figs. 4(c), 4(d), 4(g), and 4(h) with $3n_{\rm b}=n_{\rm d}=3\times10^{10}\,{\rm cm}^{-2}$, we observe

that the peak intensity of the bright excitons is three times the intensity of the dark excitons in the $n_{\rm b} = 3n_{\rm d}$ systems. Conversely, the profile of the dark excitons is three times than the value of the bright excitons in the $3n_{\rm b} = n_{\rm d}$ systems. Despite these differences, the in-plane magnetic fields can still bright the dark exciton states in all systems as shown in Fig. 4.

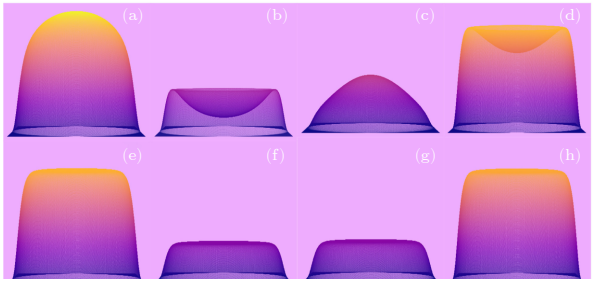

Fig. 4. Influence of the strength of the DDI on the bright and dark exciton BEC states at the K valley in a WSe_2 ML, induced by different densities of excitons. We show the normalized density $\eta = \rho/N$ profiles of bright excitons [(a), (e), (c), (g)] and dark excitons [(b), (f), (d), (h)]. We set the different strengths of the in-plane magnetic fields $B_0 = 0.00\,\mathrm{T}$ in the first row, $B_0 = 0.80\,\mathrm{T}$ in the second row. The fixed average densities of bright and dark exciton BEC states are $n_{\rm b} = 3n_{\rm d} = 3\times10^{10}\,\mathrm{cm}^{-2}$ in [(a), (b), (e), (f)] and $3n_{\rm b} = n_{\rm d} = 3\times10^{10}\,\mathrm{cm}^{-2}$ in [(c), (d), (g), (h)]. The radius of the WSe_2 ML is $R_0 = 0.3\,\mu\mathrm{m}$.

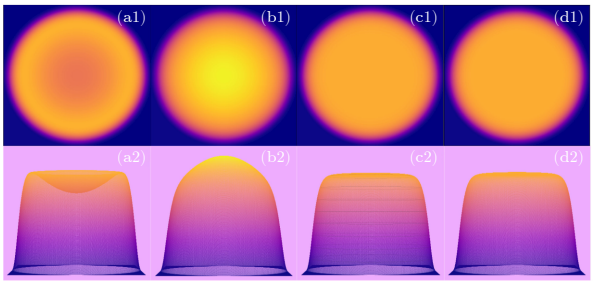

Fig. 5. Influence of materials of TMDC-MLs on exciton BEC states at the K valley in the $MoSe_2$ MLs. We show the normalized density $\eta = \rho/N$ (first row) and the density profiles (second row) of bright excitons [(a1), (a2), (c1), (c2)] and dark excitons [(b1), (b2), (d1), (d2)]. We set the different strengths of the in-plane magnetic fields $B_0 = 0.00\,\mathrm{T}$ [(a1), (a2), (b1), (b2)] and $B_0 = 0.80\,\mathrm{T}$ [(c1), (c2), (d1), (d2)]. The fixed average densities of bright and dark exciton BEC states are $n_{\rm b(d)} = 10^{10}\,\mathrm{cm}^{-2}$. The radius of the WSe_2 ML is $R_0 = 0.3\,\mu\mathrm{m}$.

In our calculations, we have utilized WSe_2 MLs to demonstrate the mixing of the bright and dark exciton BEC states under the in-plane magnetic fields. Our method can also apply to other TMDC-MLs. We explore the difference of the density distributions and phases of the exciton BEC states for MoS_2, $MoSe_2$, WS_2 and WSe_2. The parameters we used for these materials are listed in Table 1. Here, we show the density distributions and the density profiles of bright and dark exciton BEC states in the $MoSe_2$ MLs in Fig. 5. The situation of the MoS_2 MLs is similar to $MoSe_2$ MLs, and WS_2 MLs is same as WSe_2 MLs. Compared with WSe_2 MLs, the hole appears in bright exciton BEC states, rather than in dark states. The influence of DDI on the state of bright and dark excitonic BEC does not change the particle number density but alters its distribution. The repulsive interaction of DDI, which shifts the higher energy band upwards, leads to a convex shape in the exciton BEC state. Conversely, its downward polarizing effect on the lower energy band results in a concave shape in the exciton BEC state. In WS_2 and WSe_2, since $\Delta_{\rm bd} = E_{\rm d} - E_{\rm b} < 0$, the energy of dark excitons is lower than that of bright excitons, causing the DDI downward polarization to affect the dark exciton BEC state, creating a concave shape. In contrast, in MoS_2 and $MoSe_2$, where $\Delta_{\rm bd} = E_{\rm d} - E_{\rm b} > 0$, the energy of dark excitons is greater than that of bright excitons, causing the DDI downward polarization to affect the bright exciton BEC state, also resulting in a concave shape.

Table 1. Parameters of excitons in TMDC-MLs. The two conduction band electron masses are $m_{\rm e1}$ and $m_{\rm e2}$, the hole mass is $m_{\rm h1}$ [49] (m_0 is the free electron mass). The bright-dark splitting $\Delta_{\rm bd}$ is derived from the spin splitting in the conduction. The monolayer thickness d_0 is taken from Ref. [49] and the screening length bands $r_0 = 2\pi\chi_{\rm 2D}$ are taken from Ref. [50]. The critical temperature $T_{\rm c}$ is taken from Ref. [27].

	MoS_2	$MoSe_2$	WS_2	WSe_2
$m_{\rm e1}/m_0$	0.47	0.58	0.27	0.29
$m_{\rm e2}/m_0$	0.44	0.50	0.36	0.40
$m_{\rm h1}/m_0$	0.54	0.60	0.36	0.36
$\Delta_{\rm bd}$ (meV)	3	20	−31	−37
$\chi_{\rm 2D}$ (Å)	6.60	8.23	6.03	7.18
d_0 (Å)	3.17	3.335	3.14	3.34
$T_{\rm c}$ (K)	112	94	149	141

In our study, we have also focused on the critical temperature of exciton BEC states in these TMDC-MLs.[27] It is worth noting that these dark exciton BEC states enhanced by the in-plane magnetic fields can be observed even at high temperature. This phenomenon is attributed to the small Bohr radius of excitons in TMDC-MLs, which results in the high average exciton density $n_{\rm b(d)}$ and the enhancement Coulomb interaction in TMDC-MLs, leading to a high critical temperature $T_{\rm c}$ for the condensation process. For example, a WSe_2 with radius of $0.1\,\mu\mathrm{m}$ has $T_{\rm c} = 141\,\mathrm{K}$,[27] well beyond the temperature zone of liquid nitrogen, when the exciton density $n_{\rm c} = 8.0\times10^{12}\,\mathrm{cm}^{-2}$ (the ionization limit given in Ref. [52]). The critical temperatures of the other three materials are listed in Table 1. It can be seen that they are all in the temperature range of liquid nitrogen.

In summary, we have studied the exciton BEC states in TMDC-MLs under in-plane magnetic fields. The in-plane magnetic fields mix bright and dark excitons and have greatly impacted on the density distribution of exciton BEC states. We find that the bright exciton BEC states can mix the two spin levels in CB because of Zeeman effect and hence give optoelectronic activity in dark exciton BEC ground states in all of the studied systems by adding the in-plane magnetic fields. We also find these kind of effects in MoS_2, $MoSe_2$, WS_2, and WSe_2 under

the in-plane magnetic fields. The competition between the DDI arising from the long-range Coulomb interaction and the Zeeman effect induced by the in-plane magnetic fields can effectively regulate the formation of dark exciton BEC states. This means that the competitive mechanism allows us to utilize exciton concentration and the in-plane magnetic fields to adjust the strength of the dark exciton BEC states in TMDC-MLs. Our research may contribute to the advancement of the BEC research in practical application in TMDC-MLs, and provide a feasible method for achieving high temperature BEC states.

Acknowledgments. This work was supported by the National Natural Science Foundation of China (Grant Nos. 92265203 and 11974340), the Strategic Priority Research Program of the Chinese Academy of Sciences (Grant Nos. XDB0460000, XDB28000000, and XDPB22), the Chinese Academy of Sciences (Grant No. QYZDJ-SSW-SYS001), and the National Key R&D Program of China (Grant No. 2018YFA0306101).

References

[1] Bose 1924 *Z. Phys.* **26** 178
[2] Einstein A 1924 *Sitzungsber. Kgl. Preuss. Akad. Wiss.* **18** 261
[3] Laussy F P, Kavokin A V, and Shelykh I A 2010 *Phys. Rev. Lett.* **104** 106402
[4] Allen J F and Misener A D 1938 *Nature* **141** 75
[5] Anderson M H, Ensher J R, Matthews M R, Wieman C E, and Cornell E A 1995 *Science* **269** 198
[6] Meng Z, Wang L, Han W, Liu F, Wen K, Gao C, Wang P, Chin C, and Zhang J 2023 *Nature* **615** 231
[7] Zapf V, Jaime M, and Batista C D 2014 *Rev. Mod. Phys.* **86** 563
[8] Butov L V, Zrenner A, Abstreiter G, Böhm G, and Weimann G 1994 *Phys. Rev. Lett.* **73** 304
[9] Snoke D, Denev S, Liu Y, Pfeiffer L, and West K 2002 *Nature* **418** 754
[10] Fukuzawa T, Mendez E E, and Hong J M 1990 *Phys. Rev. Lett.* **64** 3066
[11] Butov L V 2003 *Solid State Commun.* **127** 89
[12] Zhu B, Chen X, and Cui X 2015 *Sci. Rep.* **5** 9218
[13] Chernikov A, Berkelbach T C, Hill H M, Rigosi A, Li Y L, Aslan B, Reichman D R, Hybertsen M S, and Heinz T F 2014 *Phys. Rev. Lett.* **113** 076802
[14] Song Y K, Jia C J, Xiong H Y *et al.* 2023 *Nat. Commun.* **14** 1116
[15] Fogler M M, Butov L V, and Novoselov K S 2014 *Nat. Commun.* **5** 4555
[16] Xiao D, Liu G B, Feng W, Xu X, and Yao W 2012 *Phys. Rev. Lett.* **108** 196802
[17] Zhu Z Y, Cheng Y C, and Schwingenschlögl U 2011 *Phys. Rev. B* **84** 153402
[18] Kośmider K, González J W, and Fernández-Rossier J 2013 *Phys. Rev. B* **88** 245436
[19] Ugeda M M, Bradley A J, Shi S F, da Jornada F H, Zhang Y, Qiu D Y, Ruan W, Mo S K, Hussain Z, Shen Z X, Wang F, Louie S G, and Crommie M F 2014 *Nat. Mater.* **13** 1091
[20] Mak K F, Lee C, Hone J, Shan J, and Heinz T F 2010 *Phys. Rev. Lett.* **105** 136805
[21] Blundo E, Felici M, Yildirim T, Pettinari G, Tedeschi D, Miriametro A, Liu B, Ma W, Lu Y, and Polimeni A 2020 *Phys. Rev. Res.* **2** 012024
[22] Echeverry J P, Urbaszek B, Amand T, Marie X, and Gerber I C 2016 *Phys. Rev. B* **93** 121107
[23] Palummo M, Bernardi M, and Grossman J C 2015 *Nano Lett.* **15** 2794
[24] Ye Z, Cao T, O'Brien K, Zhu H, Yin X, Wang Y, Louie S G, and Zhang X 2014 *Nature* **513** 214
[25] Kishida H, Nagasawa Y, Imamura S, and Nakamura A 2008 *Phys. Rev. Lett.* **100** 097401
[26] Zhang X X, You Y, Zhao S Y F, and Heinz T F 2015 *Phys. Rev. Lett.* **115** 257403
[27] Chen Y, Huang Y, Lou W, Cai Y, and Chang K 2020 *Phys. Rev. B* **102** 165413
[28] Molas M R, Faugeras C, Slobodeniuk A O, Nogajewski K, Bartos M, Basko D M, and Potemski M 2017 *2D Mater.* **4** 021003
[29] Slobodeniuk A O and Basko D M 2016 *2D Mater.* **3** 035009
[30] Rainer G, Smoliner J, Gornik E, Böhm G, and Weimann G 1995 *Phys. Rev. B* **51** 17642
[31] Camenzind L C, Yu L, Stano P, Zimmerman J D, Gossard A C, Loss D, and Zumbühl D M 2019 *Phys. Rev. Lett.* **122** 207701
[32] Dey P, Yang L, Robert C, Wang G, Urbaszek B, Marie X, and Crooker S A 2017 *Phys. Rev. Lett.* **119** 137401
[33] Kapuściński P, Delhomme A, Vaclavkova D, Slobodeniuk A O, Grzeszczyk M, Bartos M, Watanabe K, Taniguchi T, Faugeras C, and Potemski M 2021 *Commun. Phys.* **4** 186
[34] Robert C, Han B, Kapuscinski P, Delhomme A, Faugeras C, Amand T, Molas M R, Bartos M, Watanabe K, Taniguchi T, Urbaszek B, Potemski M, and Marie X 2020 *Nat. Commun.* **11** 4037
[35] He W Y, Zhou B T, He J J, Yuan N F Q, Zhang T, and Law K T 2018 *Commun. Phys.* **1** 40
[36] Bondarev I V and Lozovik Y E 2022 *Commun. Phys.* **5** 315
[37] Sethi G, Zhou Y, Zhu L, Yang L, and Liu F 2021 *Phys. Rev. Lett.* **126** 196403
[38] Sethi G, Cuma M, and Liu F 2023 *Phys. Rev. Lett.* **130** 186401
[39] Keldysh L V 1979 *JETP Lett.* **29** 716
[40] Hu H, Ramachandhran B, Pu H, and Liu X J 2012 *Phys. Rev. Lett.* **108** 010402
[41] Zhang Y, Mao L, and Zhang C 2012 *Phys. Rev. Lett.* **108** 035302
[42] Cai Y, Yuan Y, Rosenkranz M, Pu H, and Bao W 2018 *Phys. Rev. A* **98** 023610
[43] Bao W and Cai Y 2015 *SIAM J. Appl. Math.* **75** 492
[44] Bhat I A, Mithun T, and Dey B 2023 *Phys. Rev. E* **107** 044210
[45] Cai Y, Rosenkranz M, Lei Z, and Bao W 2010 *Phys. Rev. A* **82** 043623
[46] Shi Z and Huang G 2023 *Phys. Rev. E* **107** 024214
[47] Edmonds M and Nitta M 2020 *Phys. Rev. A* **102** 011303
[48] Bao W and Cai Y 2018 *Commun. Comput. Phys.* **24** 899
[49] Kormányos A, Burkard G, Gmitra M, Fabian J, Zólyomi V, Drummond N D, and Fal'ko V 2015 *2D Mater.* **2** 022001; Corrigendum: [2015 *2D Mater.* **2** 049501]
[50] Berkelbach T C, Hybertsen M S, and Reichman D R 2013 *Phys. Rev. B* **88** 045318
[51] Naraschewski M, Wallis H, Schenzle A, Cirac J I, and Zoller P 1996 *Phys. Rev. A* **54** 2185
[52] Chernikov A, van der Zande A M, Hill H M, Rigosi A F, Velauthapillai A, Hone J, and Heinz T F 2015 *Phys. Rev. Lett.* **115** 126802